Energy Loading Effects in the Scaling of Atomic Xenon Lasers

MIEKO OHWA AND MARK J. KUSHNER, SENIOR MEMBER, IEEE

Abstract—**The intrinsic power efficiency of the atomic xenon ($5d \rightarrow 6p$) infrared (1.73–3.65 μm) laser is sensitive to the rate of pumping due to electron collision mixing of the laser levels. Long duration pumping at moderate power deposition may therefore result in higher energy efficiencies than pumping at higher powers. In this paper we examine the consequences of high energy deposition (100's J/1 atm) during long pumping pulses (100's μs) on the intrinsic power and energy efficiency and optimum power deposition of the atomic xenon laser. The dominant effect of high energy loading, gas heating, causes an increase in the electron density and therefore an increase in the electron collision mixing of the laser levels. The optimum power deposition for a given gas density therefore shifts to lower values with increasing gas temperature. For sufficiently long pumping pulses, nonuniform gas heating results in convection and rarification of highly pumped regions. The optimum power deposition therefore shifts to even lower values as the length of the pumping pulse increases. As a result, laser efficiency depends on the spatial distribution of power deposition as well as its magnitude.**

I. INTRODUCTION

THE atomic xenon laser operates in the near infrared on transitions ranging from 1.73 to 3.65 μm (see Fig. 1). The transitions having the highest efficiency are between the $5d$ and $6p$ manifolds [1]–[6]. The laser is typically operated in gas mixtures consisting of a small fraction of xenon (less than a few percent) in rare gas buffers at pressures of 0.5–5 atm. Laser oscillation has been obtained in Ar–Xe [1]–[6], He–Xe [1], [3], Kr–Xe [1], Ne–Ar–Xe [9], and He–Ar–Xe [4], [9] mixtures. The highest efficiencies have been obtained in Ar–Xe mixtures. Using electron beam (e beam), [1]–[3], [5], [9], e-beam sustained discharge [1]–[3], [10], self-sustained discharge [11]–[12], and fission fragment excitation [4], intrinsic laser efficiencies in excess of 5% have been recorded [1]–[4]. This performance is impressive considering that the quantum efficiency of the 1.73 μm transition ($5d[3/2]_1 \rightarrow 6p[5/2]_2$), which is the dominant transition in optimized Ar–Xe mixtures, is ≈7% based on excitation from the ground state. Under these conditions, the $5d$ manifold is dominantly excited by a collisional radiative cascade following dissociative recombination of $ArXe^+$ (see below). These high laser efficiencies can only be reasonably explained by there being a large amount of power being recirculated between the xenon metastable levels ($6s$) and the ion in a process commonly called electroionization [1]–[3].

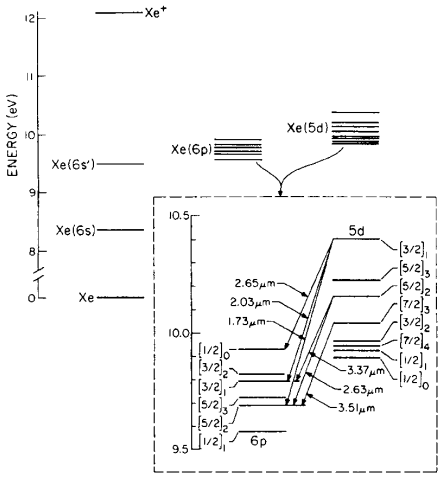

Fig. 1. Energy levels of the $6p$ and $5d$ manifolds of atomic xenon showing the dominant laser lines obtained in e-beam-pumped Ar–Xe gas mixtures.

The inversion mechanism for e-beam pumping of the atomic xenon laser using Ar–Xe mixtures has been widely studied both experimentally [1]–[6], [8]–[12] and theoretically [7], [13]. When operating with near optimum pumping conditions the 1.73 μm ($5p[3/2]_1 \rightarrow 6p[5/2]_2$) transition carries 0.7–0.9 of the total laser power while the 2.63 μm transition ($5d[5/2]_2 \rightarrow 6p[5/2]_2$) carries the majority of the remaining power. As a result of those studies, it has been hypothesized that a rapid collisional-radiative cascade following dissociative recombination of $ArXe^+$ efficiently populates the $5d$ manifold, and the $5d[3/2]_1$ level in particular [1], [5], [7]. Quenching of the common lower laser level of the 1.73 and 2.63 μm transitions ($6p[5/2]_2$) by collisions with argon is sufficiently fast that there is little competition between these lines. Both lines may simultaneously oscillate. The 2.03 μm ($5d[3/2]_1 \rightarrow 6p[3/2]_1$) transition shares the same upper laser level as the 1.73 μm transition, has the higher oscillator strength, and is the dominant laser line in gas mixtures not having a large fraction of Ar. In Ar–Xe mixtures, however, favorable quenching

Manuscript received December 6, 1989; revised March 6, 1990. This work was supported by Sandia National Laboratories, Albuquerque, NM, and by the National Science Foundation under Grants ECS 88-15781 and CBT 88-03170.

M. Ohwa was with the Department of Electrical and Computer Engineering, University of Illinois, Urbana, IL 61820. She is now with the Department of Electrical Engineering, Keio University, Kohoku-Ku, Yokohama-shi 223, Japan.

M. J. Kushner is with the Department of Electrical and Computer Engineering, University of Illinois, Urbana, IL 61820.

IEEE Log Number 9037372.

of the $6p[5/2]_2$ level allows the 1.73 μm transition to oscillate, thereby saturating the $5d[3/2]_1$ level and preventing the 2.03 μm transition from oscillating.

The $6p$ manifold is tightly coupled to the $6s$ and $5d$ manifolds by electron collisions. These collisions effectively mix the $6s$ and $6p$ manifolds, and the $6p$ and $5s$ manifolds. Since the upper laser levels are populated by a recombination cascade, and the lower laser levels are dominantly emptied by radiation or heavy particle collisions, electron collision mixing (ECM) of the $6s$, $6p$, and $5d$ manifolds is generally detrimental to the laser's performance [7]. For example, ECM of the $6p$ and $6s$ manifolds contributes to quenching of the inversion when the population of the $6s$ manifold increases at high Xe densities although it is not the dominant process [14]. Similarly, at high-power deposition, or high electron density, ECM between the $5d$ and $6p$ manifolds also reduces the population inversion. In a previous work [7] we showed that the optimum power deposition in Ar–Xe mixtures, based on the steady-state intrinsic laser efficiency, is that value for which the fractional ionization f_I is $2\text{–}3 \cdot 10^{-6}$. This value results from a balance between heavy particle quenching of the $6p$ manifold and ECM of the $6p$ and $5d$ manifolds. These results suggest that high specific laser energy can be obtained by pumping at moderate power deposition for long periods provided that this value of f_I is not exceeded. Under pumping conditions where ECM of the $5d$ and $6p$ manifolds is important, laser oscillation has been found to terminate before the end of the pumping pulse [7]–[9]. These observations suggest that the electron density increases during the pumping pulse significantly above the value where $f_I = 2\text{–}3 \cdot 10^{-6}$ and ECM dominates. We call the electron density at which ECM quenches laser oscillation the critical electron density n_c. This value corresponds to $f_I \approx 0.8 - 1.0 \cdot 10^{-5}$.

As we will discuss below, the increase in the gas temperature T_g experienced at high energy loading increases the electron density even though the power deposition is constant. As a result, a laser initially operating with an electron density near n_c (i.e., at high power deposition) can tolerate a smaller increase in gas temperature than a laser initially operating with an electron density significantly less than n_c (i.e., at low power deposition). There is, then, a relationship between energy loading, power deposition, and maximum laser pulse length. Patterson *et al.* [8], [9] performed parametric studies of the dependence of laser intensity and laser pulse width on power deposition in an e-beam-pumped xenon laser using a 1 atm gas mixture (Ar–Xe = 99.5–0.5). The duration of the e beam was 1 ms. They found that the laser often terminated prematurely (prior to the end of pumping). The energy deposition corresponding to the time at which the 1.73 μm transition terminated for various power depositions was fairly constant at ≈ 160 J/L^{-1}, although the peak laser intensity increased with increasing power deposition [8].

In this paper we examine the consequences of high-energy loading of the atomic xenon laser as is required to obtain high laser pulse energies. In particular we examine how gas heating resulting from high-energy loading may limit specific laser output energy. Our discussion will be based on results from a model for the e-beam-pumped atomic xenon laser using Ar–Xe mixtures, and comparing those results with experiments. We find that at high-energy loading, laser oscillation can be quenched by strong electron collision mixing (ECM) between the laser levels even though laser oscillation can be sustained at lower values of energy deposition. This results from the fact that the electron density and hence electron collision mixing between laser levels increases with increasing gas temperature while the rate of pumping is a constant. We also find that convection caused by gas heating increases the fractional ionization in the higher pumped and rarified regions. As a result, the duration of the laser pulse depends on the spatial distribution of power deposition as well as its magnitude.

In Section II, high-temperature kinetics in the xenon laser are discussed followed by a description of our model in Section III. General scaling relationships for laser efficiency during high-energy loading are presented in Section IV. Hydrodynamic effects resulting from nonuniform power deposition and how they relate to ECM of the laser levels are discussed in Section V. Our concluding remarks are in Section VI.

II. High Temperature and High-Energy Loading Effects

Ignoring changes in medium uniformity caused by convection, high-energy loading of gas lasers basically only changes the gas temperature. For example, with a power deposition of 100's of W/(cm^3 · atm) over a time of 100's μs netting an energy deposition of 10's of J/(L · atm) the gas temperature increases by 100's of K. The increase in gas temperature increases the rate of endothermic heavy particle quenching reactions, such as $\mathrm{Ar} + \mathrm{Xe}(6p[3/2]_1) \rightarrow \mathrm{Ar} + \mathrm{Xe}(6p[3/2]_2)$. Another important consequence of gas heating is that the rate coefficients for three-body association reactions (e.g., $\mathrm{Ar} + \mathrm{Xe}^+ + M \rightarrow \mathrm{ArXe}^+ + M$) and dissociative recombination (e.g., $\mathrm{ArXe}^+ + e \rightarrow \mathrm{Ar} + \mathrm{Xe}^{**}$) generally decrease with increasing gas temperature [15], [16]. For the conditions of interest (>0.5 atm), dissociative recombination is the dominant electron loss mechanism. The rate of ionization in an e-beam-pumped plasma is approximately P/W, where P is the power deposition and W is the amount of energy required to create an electron–ion pair. This rate, unlike that for recombination, is not a function of gas temperature. The balance between ionization and recombination, though, must always hold. That is

$$\frac{P}{W} = k_r n_e M_2^+ \tag{1}$$

where k_r is the rate constant for dissociative recombination and M_2^+ is the density of dimer ions. Since both k_r and M_2^+ decrease with increasing gas temperature then n_e must increase.

To estimate the effects of gas heating on the electron density, and on the fraction of ions which are monomers (denoted M^+) or dimers, we can write the simplified balance equations

$$\frac{\partial[M^+]}{\partial t} = \frac{P}{W} - [M^+][M]^2 k_d = 0 \quad (2a)$$

$$\frac{\partial[M_2^+]}{\partial t} = [M^+][M]^2 k_d - [e][M_2^+]k_r = 0 \quad (2b)$$

where M is any third body, and the electron density $[e] = [M^+] + [M_2^+]$. In writing (2a) we have assumed that monomer ions are formed by ionization from the beam and lost by dimerization to form M_2^+ with rate coefficient k_d, but do not otherwise recombine. The terms in (2b) for $[M_2^+]$ are for dimerization and dissociative recombination. This estimate represents a lower limit for the electron density since multistep ionization processes have been ignored. Representative rate coefficients and their temperature dependencies are [7] $k_d = 1 \cdot 10^{-31} \cdot (300\ K/T_g)^{3/2}\ \mathrm{cm^6\ s^{-1}}$ and $k_r = 3.6 \cdot 10^{-7} \cdot (1 - \exp(-180\ K/T_g))\ \mathrm{cm^3\ s^{-1}}$.

Since dissociative recombination of diatomic ions is both the dominant electron loss mechanism and the dominant pumping mechanism for the upper laser level, the rate of populating the upper laser level is basically a constant for a given power deposition regardless of gas temperature. As the electron density increases with increasing gas temperature at constant power deposition, however, ECM of the laser levels increases with no increase in net pumping. If the electron density increases to a value greater than n_c as a result of energy loading. ECM may decrease the intrinsic power efficiency or terminate laser oscillation. If the increase in electron density remains well below n_c, the increase in ECM of the laser levels may in fact, be beneficial for oscillation on a particular transition. Therefore, the intrinsic power efficiency for a given power deposition can shift to higher or lower values due to the increase in electron number density, depending upon whether n_c is closely approached or not.

In addition to these local kinetic effects, the time scales of interest (100's of μs to a few ms) are long enough for convection of the gas caused by nonuniform gas heating to be important. In these cases, the gas number density in the higher pumped region decreases due to rarification caused by the convection. If the rate of power deposition does not proportionally decrease with the decrease in gas density, as is the case with e-beam pumping using a λ geometry [8], [9], [17], the fractional ionization will increase in the rarified regions. This leads to an even higher rate of ECM, and a faster rate of approach of the electron density towards n_c. For these conditions, the duration of the laser pulse can also depend on the spatial distribution of power deposition as well as its magnitude.

III. Modeling the Effects of High-Energy Loading

The kinetics and optical time scales ($<$ 100's of ns) in the Xe laser are small compared to the hydrodynamic time scale (tens of μs). Based on these differing time scales, the instantaneous laser efficiency can be approximated as being in quasi-equilibrium with the local pumping conditions. In this approximation, the instantaneous intrinsic laser efficiency η_I can be characterized by gas mixture, laser cavity parameters, and the local values of gas number density, power deposition, and gas temperature.

Taking advantage of these differing time scales, we have formulated a model to calculate laser output power as a function of position and time which is both computationally expedient and accounts for hydrodynamic effects. In this model, we integrate the conservation equations for gas density, energy, and momentum to obtain the temporally and spatially dependent profiles of gas number density and gas temperature. These equations are

$$\frac{\partial N}{\partial t} = -\nabla \cdot \vec{v} N \quad (3)$$

$$\frac{\partial(\rho \vec{v})}{\partial t} = -\vec{\nabla} p - \vec{\nabla} \cdot \rho \vec{v} \vec{v} - \frac{\rho \vec{v}}{\tau} \quad (4)$$

$$\frac{\partial\left(\frac{3}{2} N k T_g\right)}{\partial t} = P - \nabla \cdot \vec{v}\left(\tfrac{3}{2} N k T_g\right) + \nabla \cdot \kappa \nabla T_g \quad (5)$$

where N is the gas number density, $\vec{v}$ is the convective velocity, ρ is the gas mass density, $p = NkT_g$ is the thermodynamic pressure, P is the power deposition, and κ is the thermal conductivity. τ is a viscous damping time chosen to improve the numerical stability of the solution, but does not otherwise impact the results. The power deposition, $P(\vec{r}, t)$ is a specified function. Given the differing time scales, we assume that the local intrinsic laser power efficiency is a function of the local fractional ionization and gas temperature for a given gas number density and mixture. The laser efficiency is separatedly calculated using the model described below. It is parameterized as a function of these values, and entered into a lookup table. During execution of the model, the local instantaneous laser power is calculated from the product $\eta_I P(\vec{r}, t)$, where η_I is obtained by interpolating the lookup table.

The kinetics model we used to obtain η_I is the same as that described in [7]. The framework of the model mechanically differs little from conventional models of e-beam-pumped excimer lasers. Because of the importance of the differences in excitation and quenching of individual levels in the $6p$ and $5d$ manifolds with respect to the performance of the laser, we included the individual levels of the $6p$ and $5d$ manifolds of xenon in the model in addition to the lumped states Xe*($6s$), Xe*($6s'$), Xe($7s/7p$), and Xe** (higher radiating states). The laser fluxes for transitions at 1.73, 2.63, 2.65, 3.37, and 2.03 μm are also included in the model.

IV. Model Results for the High-Temperature Kinetics of Argon–Xenon Lasers

In this section we will discuss results from our model for the quasi-steady state intrinsic power efficiency of the

atomic xenon laser in Ar–Xe mixtures. These results will be presented as a function of energy loadings of from tens to 100's of J/(L · atm). These loadings correspond to increases in gas temperature of 100's of K. Hydrodynamics effects, ignored in this section, will be discussed below. The intrinsic laser power efficiencies cited here were obtained by setting an initial gas temperature corresponding to a specific energy loading and then integrating the rate equations for the species in the zero-dimensional kinetics model until reaching a steady state. The steady state is reached in a short enough time that no additional gas heating is experienced.

For the results discussed in this and the following section, we modeled a Xe laser operating with a gas mixture of Ar–Xe = 99.5–0.5 at a pressure of 1 atm. These operating conditions were chosen because the highest intrinsic laser efficiency was predicted to occur near 1 atm, [7] operating at atmospheric pressure is attractive when using a large aperture, and experimental data is available for these parameters [8], [9]. The resonator consists of a cavity length of 1 m, total reflector, and an output mirror which has 50% reflectivity for all wavelengths of interest. The gain length is 50 cm.

As shown elsewhere [7], the optimum power deposition with respect to laser efficiency at 1 atm and 300 K is ≈ 500 W/cm^3. At power depositions of ≥ 500 W/cm^3, the intrinsic power efficiency rapidly decreases because of ECM of the laser levels. This occurs as the electron density approaches and surpasses n_c, which for these conditions is approximately $2 \cdot 10^{14}$ cm^{-3}. The effects of energy loading are manifested by the fact that the electron density is an increasing function of gas temperature.

The quasi-steady-state intrinsic laser power efficiency as a function of energy loading is shown for various power depositions in Fig. 2. The quasi-steady-state electron densities for these conditions are shown in Fig. 3. Results from the simple scaling for $[e]$ obtained from (2) are shown in Fig. 3(a) while those from the detailed model are shown in Fig. 3(b). The gas temperatures (initial values 300 K) corresponding to the indicated energy loadings are also shown in the figures. When the power deposition is held constant, the rate of populating the upper laser level due to dissociative recombination is also virtually constant since the rate of recombination simply balances ionization. As k_r decreases with increasing energy loading, however, the electron number density increases to keep the total rate of recombination a constant and equal to the ionization rate, as shown in Fig. 3. This increase in electron density results in an increase in the ECM and quenching of the laser levels, and a decrease in laser efficiency. When the electron density exceeds the critical value above which ECM dominates, oscillation cannot be sustained and the laser terminates. At a power deposition of 1 kW/cm^3, the energy deposition at which the laser oscillation terminates is less than 100 J · L^{-1}, while at a power deposition of 100 W/cm^3 laser oscillation does not terminate until an energy deposition of >1 kJ · L^{-1}. This trend results from the smaller fractional increase in

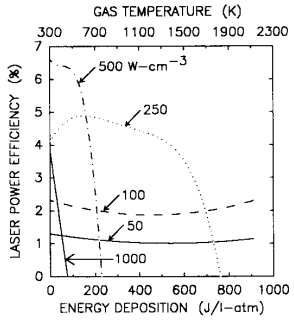

Fig. 2. Quasi-steady-state laser power efficiencies (laser power–power deposition) as a function of energy deposition for different values of power deposition in an e-beam-pumped laser. The gas mixture is Ar–Xe = 99.5/0.5 at 1 atm. The gas temperature corresponding to the indicated energy deposition is shown on the top scale. Laser oscillation is quenched due to an increase in electron density, and hence electron collision mixing, as the gas temperature increases.

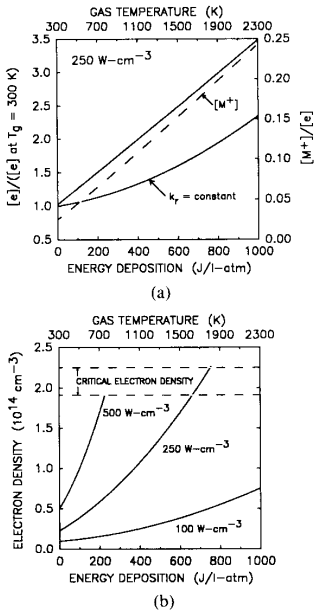

Fig. 3. Quasi-steady-state electron densities for different values of power deposition for the conditions of Fig. 2. (a) Electron density normalized by its value at T_g = 300 K as obtained with the simple scaling from (2). The lower curve was obtained while keeping k_r a constant. Also shown is the fraction of ions which are monomers M^+. (b) Results obtained from the detailed kinetics model. The range of the critical electron density, above which laser oscillation is quenched, is shown between the dashed lines. The critical electron density corresponds to a fractional ionization of $0.8 - 1.0 \cdot 10^{-5}$.

electron density required to surpass n_c at the higher pump rates. The small increase in laser efficiency found at high gas temperatures for a pump rate of 100 W/cm^{-3} is a consequence of more favorable quenching of the lower laser levels resulting from the increasing rate of endothermic reactions.

Contributions to the increase in electron density resulting from changes in the rate coefficients for dissociative

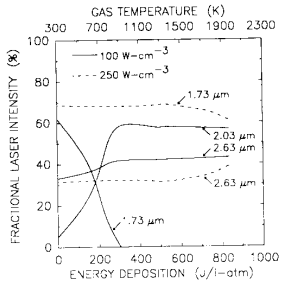

Fig. 4. Laser spectra for a power deposition of 100 and 250 W/cm^{-3} using the conditions of Fig. 2. The spectrum for 100 W/cm^{-3} is representative of low-power pumping; that for 250 W/cm^{-3} is representative of high-power pumping. The 1.73 and 2.03 μm transitions share the same upper laser level. As the rate of electron collision mixing increases with increasing energy deposition and the net gain approaches threshold, the 2.03 μm transition, which has the higher oscillator strength, begins to dominate over the 1.73 μm transitions.

recombination k_r and dimerization k_d, are shown in Fig. 3(a). Here, results from the simple scaling from (2) are plotted. The topmost curve shows the electron density, scaled by its value at 300 K, as a function of energy loading for a power deposition of 250 W/cm^{-3}. The lower curve shows the same quantity while having k_r remain a constant independent of temperature. The increase in electron density which can be attributed to the decrease in k_r is roughly equal to that which results from the decrease in the rate coefficient for dimerization. The change in the latter's value, however, significantly increases the fraction of positive ions which are monomers, also shown in Fig. 3(a).

At high values of power deposition ($\geq$250 W/cm^{-3}), the laser spectrum remains nearly constant with increasing energy loading up to the termination of the laser pulse. At lower values of power deposition, the electron density does not exceed n_c, however ECM and the increase in the rate of endothermic heavy particle quenching collisions cause a change in the spectrum of the laser, as shown in Fig. 4. As the electron density increases and net gain decreases, the 1.73 μm transition loses power to the 2.03 μm transition with which it shares the $5d[3/2]_1$ upper laser level. This spectrum corresponds to that one would obtain at low-power deposition and low gain where, due to its higher oscillator strength, the 2.03 μm line dominates.

V. Hydrodynamic Effects

Since the energy deposition at which laser oscillation is quenched depends on the specific power deposition (W/cm^3 · atm), the change in gas number density caused by gas convection driven by gas heating plays an important role in determining the laser dynamics in real systems. In this section we will discuss the effect of gas convection caused by gas heating on the spatial distribution of laser intensity in the atomic xenon laser.

The system we are modeling is patterned after the HAWK laser facility at Sandia National Laboratories [8], [9]. HAWK is a longitudinally pumped λ-type e-beam-excited laser [8], [9], [17]. The beam voltage is 1 MeV, the gas pressure is 1 atm, the gain length is 50 cm long, and the diameter of the cylindrical gas cell is 3.3 cm. The beam current injected along the axis of the gas cell may be varied to yield an average power deposition of $\leq$1 kW/cm^{-3} for times of $\leq$1 ms. (This power is the average value for a diameter of 1.8 cm centered on the axis. The peak power on the axis, as discussed below, is higher.) Due to the longitudinal pumping geometry and radial symmetry, the power deposition remains nearly constant even if rarification of the gas occurs which reduces its stopping power. This results from the fact that the lower gas pressure at axial locations closer to the source of the e beam allows more beam current to penetrate to the local position. The lower stopping power which results from a lower gas density is therefore compensated by a higher beam current. The radial distribution of power deposition may be closely approximated by

$$P(r, t) = P_0(t) \exp\left[-(r/r_0)^2\right] \qquad (6)$$

where $P_0(t)$ is the power deposition at the center of laser chamber tube and r_0 is 0.63 cm. This distribution results in there being 0.4 of the power deposited in the central 0.45 cm radius.

The computed spatial distributions of gas number density, gas temperature, and laser intensity at various times during the pumping pulse (duration 1 ms) for an average power deposition of 500 W/cm^{-3} are shown in Fig. 5. The temporal profile of the total laser power is shown in Fig. 6 for the same conditions. For these results, we have assumed that the optical mode is unaffected by changes in index of refraction of the gas caused by convection. The profile for the gas temperature closely follows that for the power deposition. The gas heating initiates convection from the highly pumped region which begins on the time scale of 100's of μs, thereby rarifying the gas near the axis. The combined effects of the increase in gas temperature and rarification result in an increase in fractional ionization. As n_c is approached and exceeded laser efficiency begins to decrease. Efficiency decreases first on the axis and later on the periphery due to the Gaussian distribution of pump power, which is peaked on axis. The position corresponding to the peak laser intensity therefore gradually shifts from the axis to outer radii [see Fig. 5(c)] while the integrated laser power decreases (see Fig. 6). At 600 μs oscillation is quenched on the axis and the laser spot becomes annular. Although the total laser output power from the aperture monotonically decreases, laser oscillation does not terminate during the 1 ms pump pulse due to there being weakly pumped regions at large radii.

The laser power and spatial intensity distribution are, logically, functions of the power deposition profile. When using a square or top-hat deposition profile having the same average power, the laser pulse terminates prior to when the power deposition profile is Gaussian (see Fig. 6). This effect results from there not being weakly pumped regions at large radii when using the top-hat profile. The

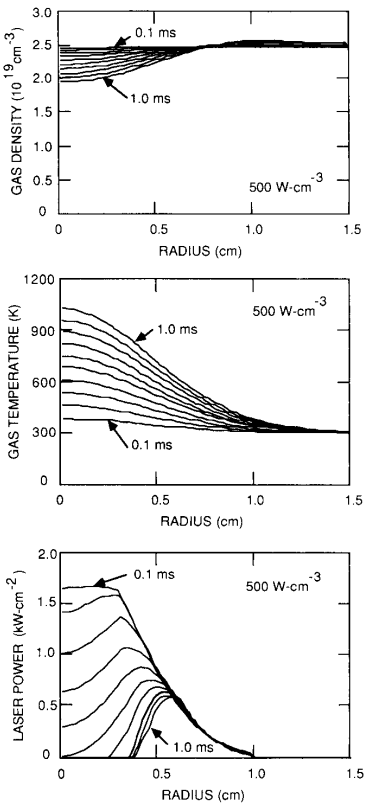

Fig. 5. Typical spatial distributions of (a) gas density, (b) gas temperature, and (c) laser intensity for an average power deposition of 500 W/cm^3 at various times during a 1 ms pumping pulse. The gas pressure is 1 atm and the gas mixture is Ar–Xe = 99.5/0.5.

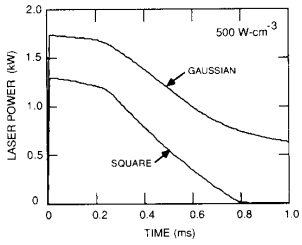

Fig. 6. Time dependence of the spatially integrated laser power for the conditions of Fig. 5 using a Gaussian power deposition profile, and for using a square or top-hat profile. Laser power decreases at late times due to increasing amounts of electron collision quenching. The low laser power at late times using the Gaussian pulse results from weakly pumped regions at large radii, which do not exist using the top-hat profile.

spot therefore remains circular and does not take on an annular shape, until very near total quenching, as shown in Fig. 7. Experiments have been performed on the HAWK facility during which the laser pulsewidth was measured as a function power deposition. Results of the experiments and values calculated by the model for the FWHM of the aperture integrated laser power are shown in Fig. 8. The laser oscillates for the entire pumping pulse

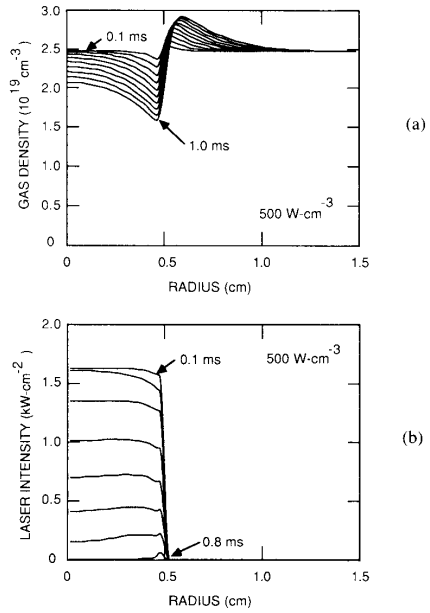

Fig. 7. Typical distributions of (a) gas density and (b) laser intensity using a square or top-hat power deposition profile. The conditions are otherwise the same as in Fig. 5. The integrated laser power is shown in Fig. 6.

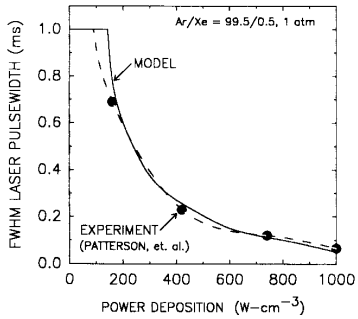

Fig. 8. Laser pulsewidth (FWHM) as a function of average power deposition using a 1 ms e-beam pulse calculated with the model and from experiments of Patterson *et al.* [9]. The conditions are the same as for Fig. 5 and correspond to those used in experiments conducted on the HAWK laser facility.

for average power depositions of <200 W/cm^{-3}. At higher power deposition, the laser prematurely terminates due to excessive ECM. The model agrees well with the experiment over the range of power deposition.

The maximum attainable laser power logically increases with increasing power deposition. The peak aperture integrated laser powers during the pumping pulse for the conditions of Fig. 8 are shown in Fig. 9. Given the decreasing length of the laser pulse but increasing peak laser power obtained with increasing power deposition, the total laser energy and laser energy efficiency will not similarly scale. The total laser energy reaches nearly a

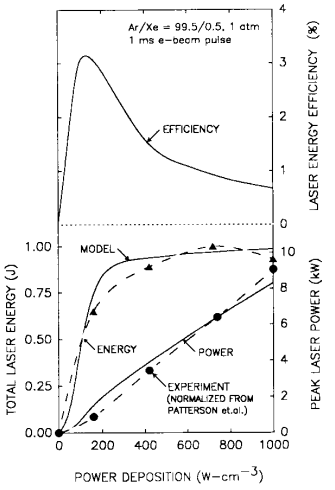

Fig. 9. Laser parameters for the conditions of Fig. 5: (top) Laser energy efficiency (laser output energy–total energy deposition) for a 1 ms *e*-beam pulse; and (bottom) maximum laser power and total laser energy. Experimental results from Patterson *et al.* ([8] and [9]) are shown for comparison. The results of the model were normalized to account for possible differences in pump profiles. The model predicts a high total laser energy by approximately 50%. Although maximum laser power increases with increasing power deposition, the laser energy reaches a maximum value at lower power deposition. The result is that the laser energy efficiency maximizes at lower values of power deposition.

maximum value at ≈ 400 W/cm^{-3} and is then almost constant at higher power depositions, as shown in Fig. 9. Experimental results from Patterson *et al.* are also shown [8], [9]. The model and experimental results were normalized to account for differences in power deposition profiles and agree well for scaling to lower powers.

The total laser energy efficiency (laser output energy–total deposition) depends upon the format of the power deposition. For example, continuing to pump after the laser terminates decreases the laser energy efficiency. For the experimental conditions we are simulating, a 1 ms pumping pulse length, the laser energy efficiency reaches a maximum value at ≈ 150 W/cm^{-3} and then decreases with increasing power deposition due to continued pumping after termination of the laser pulse. Tailoring of the pumping pulse to a length not exceeding the maximum laser pulse length is required to maximize the laser energy efficiency.

IV. Concluding Remarks

The effects of high-energy deposition (100's of J/L · atm) on the performance of high-pressure xenon lasers have been examined by computer modeling and comparing to experimental results. The dominant effect of high-energy loading is gas heating, which increases the electron density by reducing the rate of formation of dimer ions and reducing the rate constant for dissociative recombination of dimer ions. As a result of there being a critical electron density above which laser oscillation is quenched by electron collision mixing of the laser levels, laser performance degrades with increasing energy loading even though the power deposition remains constant. This effect results from the electron density approaching and surpassing the critical value. Nonuniform pumping over tens of 100's of μs may result in convection, rarification, and an increase in the fractional ionization of the gas. If as a result the electron density exceeds the critical value, laser oscillation may locally terminate. The maximum energy deposition above which oscillation is quenched by electrons decreases with increasing power deposition since the fractional increase in electron density required to exceed the critical value is smaller. These results demonstrate that laser energy, power, laser energy efficiency, and laser power efficiency may not necessarily be separately optimized. Careful tailoring of the pump pulse is required to optimize one or all of these parameters.

Acknowledgment

The authors wish to thank E. L. Patterson, P. J. Brannon, W. J. Alford, and G. N. Hays of Sandia National Laboratories for helpful discussions and access to their experimental results prior to publication.

References

[1] N. G. Basov, V. A. Danilychev, A. Yu. Dudin, D. A. Zayarnui, N. N. Ustinovskii, I. V. Kholin, and A. Yu. Chugunon, "Electron-beam-controlled atomic Xe infrared laser," *Sov. J. Quantum Electron.*, vol. 14, pp. 1158–1167, 1985.

[2] N. G. Basov, V. V. Baranov, A. Y. Chugunov, V. A. Danilychev, A. Y. Dudin, I. V. Kholin, N. N. Ustinovskii, and D. A. Zayarnyi, "60 J quasistationary electronionization laser on Xe atomic metasta-

bles," *IEEE J. Quantum Electron.*, vol. QE-21, pp. 1756-1760, 1985.
[3] S. A. Lawton, J. B. Richards, L. A. Newman, L. Specht, and T. A. DeTemple, "The high-pressure neutral infrared xenon laser," *J. Appl. Phys.*, vol. 50, pp. 3888-3898, 1979.
[4] W. J. Alford and G. N. Hays, "Measured laser parameters for reactor-pumped He/Ar/Xe and Ar/Xe lasers," *J. Appl. Phys.*, vol. 65, pp. 3760-3766, 1989.
[5] P. J. M. Peters, Q.-C. Mei, and W. J. Witteman, "Pressure-dependent optical delay time measurements in a coaxial electron beam pumped Ar: Xe laser," *Appl. Phys. Lett.*, vol. 54, 193-195, 1989.
[6] A. Suda, B. Wexler, B. Feldman, and K. Riley, "Measurements of gain, saturation, and line competition in an electron beam pumped high-pressure Ar/Xe laser," *Appl. Phys. Lett.*, vol. 54, pp. 1305-1307, 1989.
[7] M. Ohwa, T. J. Moratz, and M. J. Kushner, "Excitation mechanisms of the electron-beam-pumped atomic xenon ($5d \rightarrow 6p$) laser in Ar/Xe mixtures," *J. Appl. Phys.*, vol. 66, pp. 5131-5145, 1989.
[8] E. L. Patterson, G. E. Samlin, and P. J. Brannon, "A 1-ms electron-beam-pumped laser kinetics experiment," presented at the Conf. on Quantum Electron. and Laser Sci., Baltimore, MA, April 26, 1989.
[9] ——, "A study of an *e* beam excited atomic xenon laser at high energy loading," *IEEE J. Quantum Electron.*, vol. 26, pp. 1661-1667, Sept. 1990.
[10] A. Suda, B. L. Wexler, K. J. Riley, and B. J. Feldman, "Characteristics of the high pressure Ar-Xe laser pumped by an electron beam and an electron-beam sustained discharge," *IEEE J. Quantum Electron.*, vol. 26, pp. 911-921, May 1990.
[11] F. S. Collier, P. Labstie, M. Maillet, and M. Michon, "High-efficiency infrared xenon laser excited by a UV preionized discharge," *J. Quantum Electron.*, vol. QE-19, pp. 1129-1133, 1983.
[12] J. E. Tucker, B. L. Wexler, B. J. Feldman, and T. McClelland, "High-pressure infrared xenon laser with X-ray preionization," *IEEE Photon. Technol. Lett.*, vol. 1, pp. 193-195, 1989.
[13] K. S. Klopovskii, A. V. Luk'yanova, A. T. Rakhimov, and N. V. Suetin, "Numerical modeling of an atomic xenon laser," *Sov. J. Quantum Electron.*, vol. 19, pp. 133-137, 1989.
[14] Although electron collision mixing of the 6*s* and 6*p* manifolds contributes to quenching of oscillation at high xenon fraction, the dominant effect is believed to be quenching of $5d[3/2]$, level by collisions with xenon. See [7].
[15] T. J. Moratz, T. D. Saunders, and M. J. Kushner, "High temperature kinetics in He and Ne buffered XeF lasers: The effect on absorption," *Appl. Phys. Lett.*, vol. 54, pp. 102-104, 1989; and references cited therein.
[16] D. C. Jones, D. G. Lister, and N. D. Twiddy, "Equilibrium constant for the reaction $Xe^+ + 2\,Ar \rightleftarrows Xe\,Ar^+ + Ar$ in the temperature range 150-300 K and the dissociation energy of $Xe\,Ar^+$," *Chem. Phys. Lett.*, vol. 70, pp. 575-578, 1980.
[17] J. M. Hoffman, E. L. Patterson, and R. A. Gerber, "Energy extraction from a large-volume HF laser amplifier," *J. Appl. Phys.*, vol. 50, pp. 3861-3866, 1979.

Mieko Ohwa received the B.S., M.S., and Ph.D. degrees from Keio University, Yokohama, Japan, in 1983, 1985, and 1988, respectively. While there, she mainly studied the laser kinetics of rare-gas halide lasers and F_2 lasers.

Since 1988, she has been with the University of Illinois at Urbana-Champaign as a Postdoctoral Research Associate. Her current research interests include soft-X-ray source, nonlinear optics, and nucleation and growth of thin film.

Mark J. Kushner (S'74-M'79-SM'89), for a photograph and biography, see this issue, p. 1554.